Global Optical Potential for the Elastic Scattering of ^{6}He at Low Energies

Y. Kucuk

Department of Physics, Giresun University, Giresun, Turkey

I. Boztosun

Department of Physics, Akdeniz University, Antalya, Turkey,

T. Topel

Institute of Science, Erciyes University, Kayseri, Turkey

arXiv:0911.3991v1 [nucl-th] 20 Nov 2009

Abstract

A set of global optical potential has been derived to describe the interactions of ^{6}He at low energies. The elastic scattering angular distribution data measured so far for many systems, ranging from ^{12}C to ^{209}Bi, have been considered within the framework of the optical model in order to find a global potential set to describe the experimental data consistently. We report that very good agreement between theoretical and experimental results has been obtained with small χ^2/N values by using the derived potential set. The reaction cross section and volume integrals of the potentials have been deduced from the theoretical calculations for all studied systems at relevant energies.

PACS numbers: 24.10.Eq; 24.10.Ht; 24.50.+g; 25.60.-t; 25.70.-z

I. INTRODUCTION

Defining the structure and dynamics of the halo nuclei has been a central area for the nuclear physics in the past decades. Particularly, nuclear astrophysicists has been involved with the reaction mechanism of the short-lived exotic nuclei, which bear great importance due to the capture reactions that occurred in early universe. To get more information regarding the nature of halo nuclei and its reaction mechanism, many experiments have been carried out by using the Radioactive Ion Beams (RIB) facilities.In this respect, ^{6}He has been one of the most studied nuclei to understand the structure of the weak binding and of the large radial extent to investigate the effect of the halo structure on the reaction observables [1, 2, 3, 4, 5, 6, 7, 8, 9, 10, 11, 12, 13, 14, 15, 16, 17, 18]. In these works, the elastic scattering, the fusion and the break-up/transfer cross sections have been measured and studied theoretically for many systems at energies near the Coulomb barrier to investigate the behavior of the optical potential and the effect of break-up coupling to the reaction and the scattering mechanism. The role of the Coulomb and nuclear break-up on the fusion cross section has been attempted to be addressed by studying the interaction of ^{6}He with heavy nuclei such as ^{208}Pb, ^{209}Bi and ^{238}U [9, 10, 11, 19, 20, 21, 22, 23, 24, 25, 26, 27, 28, 29]. Different interpretations have been presented about how the break-up coupling affects the fusion process. These works have been extended from the heavy nuclei to weaker ones such as ^{27}Al, ^{64}Zn and ^{65}Cu and it has been observed that transfer and break-up cross section were more important than the fusion cross sections at energies above the Coulomb barrier for weaker systems and total cross section of the reactions induced by halo nuclei has a large value as compared the total cross section of stable nuclei reactions such as ^{4}He and ^{6}Li [30, 31, 32].

In addition to discussions about the reaction mechanism of the halo nuclei, the explanation of the measured elastic scattering angular distributions near the Coulomb barrier has been the other motivation of these studies since elastic scattering bears a great importance to provide an idea about the nuclear optical potential of the system. To observe the scattering mechanism of ^{6}He, the experimental data for many systems including light or heavy nuclei have been analyzed by using phenomenological and microscopic potentials [33, 34]. In a recent paper, Milin *et al.* [34] have studied ^{6}He+^{12}C system and they have measured the elastic and inelastic scattering as well as $2n$ transfer reaction angular distribu-

tions at E_{Lab}=18.0 MeV.They have analyzed these data by using the Woods-Saxon shaped phenomenological optical potential [34] and they were able to obtain a consistent agreement for the elastic scattering and transfer reaction data, but they were not able to obtain the inelastic 2^+ data simultaneously with the elastic and transfer channels data. The same data has been analyzed by Boztosun *et al.* [35] and they were able to obtain a simultaneous description of the elastic, inelastic and transfer reaction cross sections by deforming the long range imaginary potential within the framework of the CCBA formalism.

Studies on the elastic scattering of ^{6}He on medium mass target nuclei has been presented by some authors in previous years. Benjamim *et al.* [30] have measured the elastic scattering angular distribution of the ^{6}He+^{27}Al system with RIBRAS facility and have investigated the behavior of the total reaction cross section. They have used the São Paula Potential (SPP) to reproduce the elastic scattering data and they have extracted the reaction cross section for this system at some energies. For ^{6}He+^{64}Zn system, elastic scattering angular distributions, transfer/break-up angular distributions and fusion excitation functions have been measured at near the Coulomb barrier energies by Pietro *et al.*[31] to investigate the effects of neutron halo structure on the reaction mechanism. An optical model analysis has been performed to explain the elastic scattering data and the total reaction cross section data has been extracted from this analysis. Another reaction of ^{6}He on medium mass target is ^{6}He+^{65}Cu system. For this system, the measured elastic scattering cross section has been analyzed by using the statistical model and the reaction cross section has been obtained from the theoretical results [32].

^{6}He+^{208}Pb and ^{6}He+^{209}Bi are the examples of the systems with heavy targets, which have been studied extensively to measure elastic scattering around the Coulomb barrier energies. The ^{6}He+^{208}Pb system has been recently studied by Sánchez Benítez [29] and they have measured elastic scattering cross section at energies between 14 and 22 MeV. In this work, the experimental data have been analyzed by using the phenomenological Wood-saxon potential and the presence of the long range absorption has been reported for this system. Aguilera *et al.* [9, 10] for ^{6}He+^{209}Bi system have performed the simultaneous analysis of the elastic scattering and transfer reaction cross section at energies below the Coulomb barrier by using the optical model.

As seen from the literature, ^{6}He interactions at energies around Coulomb barrier have crucial importance in understanding the properties of exotic systems and a global potential

set is required in the theoretical analysis of the reactions. So far, many potential sets have been used either phenomenological or of the folding type to describe the elastic scattering and other scattering observables of ^{6}He nucleus. These potentials are very similar to those of the ^{6}Li potentials. Sometimes, ^{4}He potential has also been used by adjusting the radius for ^{6}He one.Although a good description of the observables by using these potentials has been obtained for individual reactions, there is no global potential that describe the elastic scattering of ^{6}He from different target nuclei consistently.

Therefore, in this paper, we aim to develop a global potential set to describe the elastic scattering of the ^{6}He nucleus from light to heavy target nuclei at low energies. In the next section, we present the optical model and introduce our global potential.The results of the theoretical analysis by using our global potential set for many systems have been presented in Section III. We conclude in Section IV.

II. OPTICAL MODEL CALCULATIONS

We have performed an extensive study for the elastic scattering of ^{6}He on different target, from ^{12}C to ^{209}Bi, for a wide energy range. We have used the optical model for the theoretical calculations and the total effective potential in the optical model consists of the Coulomb, centrifugal and nuclear potentials as

$$V_{total}(r) = V_{Nuclear}(r) + V_{Coulomb}(r) + V_{Centrifugal}(r) \tag{1}$$

In the total effective potential, the Coulomb and Centrifugal potentials are well-known. The Coulomb potential [36] due to a charge $Z_P e$ interacting with a charge $Z_T e$ distributed uniformly over a sphere of radius R_c is given by

$$V_{Coulomb}(r) = \frac{1}{4\pi\epsilon_\circ}\frac{Z_P Z_T e^2}{r}, \qquad r \geq R_c \tag{2}$$

$$= \frac{1}{4\pi\epsilon_\circ}\frac{Z_P Z_T e^2}{2R_c}(3 - \frac{r^2}{R_c^2}), \qquad r < R_c \tag{3}$$

where R_c is the Coulomb radius, taken as 1.2 fm in the calculations and Z_P and Z_T denote the charges of the projectile P and the target nuclei T respectively.

The centrifugal potential is

$$V_{Centrifugal}(r) = \frac{\hbar^2\, l\,(l+1)}{2\,\mu\, r^2} \tag{4}$$

where μ is the reduced mass of the colliding pair.

Finally, the complex $V_{Nuclear}(r)$ potential is taken to be the sum of the Woods-saxon square shaped real and Wood-Saxon shaped imaginary potentials given as

$$V_{nuclear}(r) = \frac{-V_0}{\left[1 + e^{\frac{r-R_V}{a_V}}\right]^2} + i\frac{-W_0}{1 + e^{\frac{r-R_W}{a_W}}} \tag{5}$$

Here, R_i=$r_i[A_P^{1/3} + A_T^{1/3}]$ ($i = V$ or W), where A_P and A_T are the masses of projectile and target nuclei and r_V and r_W are the radius parameters of the real and imaginary parts of the nuclear potential respectively.

By taking free parameters of the depth of the real and imaginary potential, we have investigated their radii for each part, which give the best fit for the elastic scattering cross section data. In order to perform this, we have made a χ^2 search. The radii of real (r_V) and imaginary potentials (r_W) have been varied on a grid, respectively from 0.5 to 2.0 fm, with steps of 0.1 fm in order to obtain the best fit to the data [37].The results of this systematic search are shown in Figure 1 which is a three-dimensional plot of the r_V, r_W and $1/\chi^2$, where χ^2 has the usual definition and measures the quality of the fit. In Figure 1, the best fit parameters, producing oscillating cross-sections with reasonable phase and period, correspond to low χ^2 values and peaks in the $1/\chi^2$ surface. For the four different reactions, the figures present discrete peaks (or hills) for correlated r_V and r_W values, which are best fit real and imaginary potential families and indicate that the r_V or r_W parameters cannot be varied continuously and still find equally satisfying fits. For the radius of real part (r_V), the lowest χ^2 values are generally obtained around 0.9 fm and for the radius of imaginary part (r_W), it is around 1.50 fm. The diffusion parameters have also been fixed a_V=a_W=0.7 fm for both parts of the potential.

Having obtained the best fit for all data, we have investigated the change of the depth of the real and imaginary parts and we have derived Equations 6 and 7 for the variation of the depth of the real and imaginary parts of the nuclear potential. Equations depend on the incident energy of the projectile (^{6}He) with the charge number (Z) and mass number(A) of the target.

$$V_0 = 110.1 + 2.1\,\frac{Z_T}{A_T^{1/3}} + 0.65\,E \tag{6}$$

$$W_0 = 6.0 + 0.48\,\frac{Z_T}{A_T^{1/3}} - 0.15\,E \tag{7}$$

where E is the laboratory energy of the ^{6}He and Z_T and A_T are the charge and mass numbers of the target nuclei.

For ^{6}He+^{208}Pb system, the real and imaginary potentials are shown in Figure 2 for E_{Lab}= 18.0 MeV. The sum of the nuclear, Coulomb and the centrifugal potentials is also shown in the same figure for the orbital angular momentum quantum numbers, $l = 0$ to 50. The superposition of the attractive and repulsive potentials results in the formation of a potential pocket, which the width and depth of the pocket depend on the orbital angular momentum. It is well known that this pocket is very important for the interference of the barrier and internal waves, which produces the pronounced structure in the cross-section [38, 39]. We perceive from Figure 2 that the real part is located inside the imaginary one, which shows that the long range absorption is needed to explain the interaction of ^{6}He.

III. RESULTS

We have analyzed the elastic scattering of the ^{6}He from target nuclei of the ^{12}C, ^{27}Al, ^{58}Ni, ^{64}Zn, ^{65}Cu, ^{197}Au, ^{208}Pb and ^{209}Bi for a wide energy range below 50 MeV by using the derived new optical potential set given by Eqs. 6 and 7 within the framework of the optical model.

First system we have considered is the ^{6}He+^{12}C elastic scattering, an example of the light-heavy target, and we have analyzed this system at 8.79, 9.18 and 18.0 MeV energies in the laboratory system. The experimental data for 8.79 and 9.18 have been measured by Smith *et al.* [33] and have been analyzed by using the potential parameters of ^{4}He, ^{6}Li and ^{7}Li. In their work, the angular distribution of ^{6}He has been well produced by using ^{6}Li and ^{7}Li optical potential parameters while ^{4}He parameters have not produced the data well. In our study, the elastic scattering data at these energies as well as the data at 18.0 MeV measured by Milin *et al.* [34] have been analyzed by using the new potential and a good agreement has been obtained for all energies as presented in Figure 3. When the theoretical results are compared with experimental data, we have obtained small χ^2/N values as it is seen in Table I. In the same table, we have also presented the prediction of the new potential parameters for the reaction cross section. The values are comparable with more

sophisticated CDCC or similar approaches.

Another studied system is the ^{6}He+^{27}Al reaction. Elastic scattering data of this system has been measured at energies 9.5, 11.0, 12.0, 13.4 MeV by using the RIBRAS (Radioactive Ion Beams in Brazil) facilities by Benjamim *et al.* [30].They have also analyzed the measured data theoretically by using the Sao Paulo Potential (SPP) and they have also deduced the reaction cross section from the optical model fits. They have predicted the reaction cross sections for these energies as 1110, 1257, 1300, 1327 mb, respectively. In comparing our results with these values, we see a difference of about 200 mb between the microscopic and our phenomenological potentials. The difference is due to the shape of the imaginary potential. The theoretical results of our potential for ^{6}He+^{27}Al elastic scattering and extracted reaction cross sections for each energy are given in Table I and Figure 4.

For the medium mass target, ^{58}Ni, ^{64}Zn and ^{65}Cu have been analyzed by using the optical potential parameters obtained from potential formula (Eqs. 6 and 7). These systems have been studied around the Coulomb barrier and the elastic scattering cross section have been measured by Refs. [17, 31, 32]. For ^{6}He+^{64}Zn system, the reaction cross section has been deduced as 380$\mp$60 mb for 10.0 MeV and 1450$\mp$130 mb for 13.6 MeV using the phenomenological potential set by Ref. [31]. These values are comparable with our results with a difference of around 10%. The results of our potential for the elastic scattering of these reactions and the reaction cross section values for each energy are given in Table I and Figure 5.

We have also studied the elastic scattering of ^{6}He from heavy targets such as ^{197}Au, ^{208}Pb and ^{209}Bi. For these systems, the elastic scattering angular distributions have been measured at energies near the Coulomb barrier generally. Kakuee *et al.* [12] have measured the elastic scattering cross section of ^{6}He+^{197}Au and ^{6}He+^{208}Pb at 27.0 MeV and they have analyzed the data by using the optical model. In their calculations, they have used the parameters that fit the ^{6}Li systems by both taking into account and ignoring the dipole polarizability. However, since this potential set was not adequate to fit the data, they have modified the potential by changing the depth and diffuseness of the real potential. They have shown that large imaginary diffuseness parameters are required to fit the experimental data and they have presented these results as an evidence of the long-range absorbtion mechanism. In this work, they have found the reaction cross section around 1900 mb at 27 MeV, which is estimated due to Coulomb break-up. In comparing this work with our calculations, we

observe the same results. Our potential produces the reaction cross section as 1925 mb and 1892 mb for ^{197}Au and ^{208}Pb nuclei at 27 MeV energy respectively. It also gives good results to elastic scattering with very small χ^2/N values as shown in Figure 6, Figure 7 and Table I. Beside these works, the elastic scattering cross sections of ^{6}He+^{208}Pb and ^{6}He+^{209}Bi for eleven different energies conducted in literature [9, 10, 29] have been studied and excellent agreement have been obtained for experimental data. The results for some energies are given in Figures 7 and 8.

We should point out that although the new potential set provides a consistent agreement for many systems, the potential parameters need a small modification to fit the experimental data at some energies for heavy targets. As seen in Figures 9, while the new potential predict the behavior of the cross section, it can not fit the data exactly: It is over/under-estimate the experimental data at particular cases. However, a change of the depth of the imaginary potential such as ± 5 MeV is sufficient to fit the data.

In Table I, for all reactions we have studied in this paper, we have presented the χ^2/N values, the reaction cross section values and the volume integrals produced by new potential set. For the theoretical calculations, the code Fresco [40] has been used.

IV. CONCLUSION

We have presented a new potential set by deriving a formula for the depth of the real and imaginary parts of the optical potential for ^{6}He elastic scattering at low energies. We should point out that we do not aim to obtain the best fits for the experimental data. Rather, we attempt to derive a global potential set that produces the behavior of the experimental data reasonably well. In this sense, we have analyzed almost all experimental data conducted over a wide energy range in the literature by using this potential set to show the validity of the potential in explaining the elastic scattering data and reasonable agreement has been obtained for all data with reasonable χ^2/N values.

As it may be seen from our results obtained by using the new potential parameters, one can easily use this potential set instead of using the improved parameters of the most similar nuclei such as ^{4}He, ^{6}Li and ^{7}Li as it is most commonly done. This global potential can also be extended to describe the scattering observables of other halo type nuclei which is important in providing information regarding their interaction mechanism.

Acknowledgments

This work has been supported by the Turkish Science and Research Council (TÜBİTAK) with Grant No:107T824, the Turkish Academy of Sciences (TÜBA-GEBİP) and Akdeniz University Scientific Research Projects Unit.

---

[1] J. S. Al-Khalili M. D. Cortina-Gil, P. Roussel-Chomaz, N. Alamanos, J. Barrette, W. Mittig, F. Auger, Y. Blumenfeld, J. M. Casandjian, M. Chartier, V. Fekou-Youmbi, B. Fernandez, N. Frascaria, A. Gillibert, H. Laurent, A. Lepine-Szily, N. A. Orr, V. Pascalon, J. A. Scarpaci and J. L. Sida, Phys. Lett. B **378**, 45 (1996).

[2] J. S. Al-Khalili, J. A. Tostevin and I. J. Thompson, Phys. Rev. C **54**, 1843 (1996).

[3] S. Karataglidis, P. J. Dortmans, K. Amos and C. Bennhold, Phys. Rev. C **61**, 024319 (2000).

[4] Y. Suzuki, Nucl. Phys. A **528**, 395 (1991).

[5] K. Varga, Y. Suzuki and Y. Ohbayasi, Phys. Rev. C **50**, 189 (1994).

[6] S. Funada, H. Kameyama and Y. Sakuragi, Nucl. Phys. A **575**, 93 (1994).

[7] P. Navratil, W. E. Ormand, E. Caurier and C. Bertulani, Lawrence Livemore National Laboratory, UCRL-PROC-211912, (2005).

[8] A. M. Sánchez Benítе, D. Escrig, M. A. G. Alvarez, M. V. Andres, C. Angulo, M. J. G. Borge, J. Cabrera, S. Cherubini, J. M. Espino, P. Figuera, M. Freer, J. E. Garcia-Ramos, J. Gomez-Camacho, M. Gulino, O. R. Kakuee, I. Martel, C. Metelco, A. M. Moro, J. Rahighi, K. Rusek, D. Smirnov, O. Tengblad, P. Van Duppen and V. Ziman, J. Phys. G: Nucl. Part. Phys. **31**, S1953 (2005).

[9] E. F. Aguilera, J. J. Kolata, F. M. Nunes, F. D. Becchetti, P. A. DeYoung, M. Goupell, V. Guimaraes, B. Hughey, M. Y. Lee, D. Lizcano, E. Martinez-Quiroz, A. Nowlin, T. W. O'Donnell, G. F. Peaslee, D. Peterson, P. Santi and R. White-Stevens, Phys. Rev. Lett. **84**, 5058 (2000).

[10] E. F. Aguilera, J. J. Kolata, F. D. Becchetti, P. A. DeYoung, J. D. Hinnefeld, A. Horvath, L. O. Lamm, Hye-Young Lee, D. Lizcano, E. Martinez-Quiroz, P. Mohr, T. W. ODonnell, D. A. Roberts and G. Rogachev, Phys. Rev. C **63**, 061603(R) (2001).

[11] J. J. Kolata, V. Guimaraes, D. Peterson, P. Santi, R. White-Stevens, P. A. DeYoung, G. F.

Peaslee, B. Hughey, B. Atalla, M. Kern, P. L. Jolivette, J. A. Zimmerman, M. Y. Lee, F. D. Becchetti, E. F. Aguilera, E. Martinez-Quiroz and J. D. Hinnefeld, Phys. Rev. Lett. **81**, 4580 (1998).

[12] O. R. Kakuee, M. A. G. Alvarez, M. V. Andres, S. Cherubini, T. Davinson, A. Di Pietro, W. Galster, J. Gomez-Camacho, A. M. Laird, M. Lamehi-Rachti, I. Martel, A. M. Moro, J. Rahighi, A. M. Sanchez-Benitez, A. C. Shotter, W. B. Smith, J. Vervier and P. J. Woods, Nucl. Phys. A **765**,294 (2006).

[13] O. R. Kakuee, J. Rahighi, A. M. Sanchez-Benitez, M. V. Andres, S. Cherubini, T. Davinson, W. Galster, J. Gomez-Camacho, A. M. Laird, M. Lamehi-Rachti, I. Martel, A. C. Shotter, W. B. Smith, J. Vervier and P. J. Woods, Nucl. Phys. A **728**, 339 (2003).

[14] R. Raab, Katholieke Universiteit Leuven, PhD. Thesis, (2001).

[15] L. Borowska, K. Terenetsky, V. Verbitsky and S. Fritzsche, Phys. Rev. C **76**, 034606 (2007).

[16] A. A. Korsheninnikov, E. A. Kuzmin, E. Yu. Nikolskii, C. A. Bertulani, O. V. Bochkarev, S. Fukuda, T. Kobayashi, S. Momota, B. G. Novatskii, A. A. Ogloblin, A. Ozawa, V. Pribora, I. Tanihata and K. Yoshida, Nucl. Phys. A **616**, 189 (1997).

[17] L. R. Gasques, L. C. Chamon, D. Pereira, V. Guimaraes, A. Lepine-Szily, M. A. G. Alvarez, E. S. Rossi, Jr. , C. P. Silva, B. V. Carlson, J. J. Kolata, L. Lamm, D. Peterson, P. Santi, S. Vincent, P. A. De Young and G. Peasley, Phys. Rev. C **67**, 024602 (2003).

[18] R. E. Warner, F. D. Becchetti, J. W. Janecke and D. A. Roberts, Phys. Rev. C **51**, 178 (1995).

[19] P. A. DeYoung, Patrick J. Mears, J. J. Kolata, E. F. Aguilera, F. D. Becchetti, Y. Chen, M. Cloughesy, H. Griffin, C. Guess, J. D. Hinnefeld, H. Jiang, Scott R. Jones, U. Khadka, D. Lizcano, E. Martinez-Quiroz, M. Ojaniega, G. F. Peaslee, A. Pena, J. Rieth, S. VanDenDriessche and J. A. Zimmerman, Phys. Rev. C **71**, 051601(R) (2005).

[20] M. Trotta, J. L. Sida, N. Alamanos, A. Andreyev, F. Auger, D. L. Balabanski, C. Borcea, N. Coulier, A. Drouart, D. J. C. Durand, G. Georgiev, A. Gillibert, J. D. Hinnefeld, M. Huyse, C. Jouanne, V. Lapoux, A. Lepine, A. Lumbroso, F. Marie, A. Musumarra, G. Neyens, S. Ottini1, R. Raabe, S. Ternier, P. Van Duppen, K. Vyvey, C. Volant and R. Wolski, Phys. Rev. Lett. **84**, 2342 (2000).

[21] R. Raabe, J. L. Sida, J. L. Charvet, N. Alamanos, C. Angulo, J. M. Casandjian, S. Courtin, A. Drouart, D. J. C. Durand, P. Figuera, A. Gillibert, S. Heinrich, C. Jouanne, V. Lapoux,

A. Lepine-Szily, A. Musumarra, L. Nalpas, D. Pierroutsakou, M. Romoli, K. Rusek and M. Trotta, Nature **431**, 823 (2004).

[22] J. J. Kolata, H. Amro, F. D. Becchetti, J. A. Brown, P. A. DeYoung, M. Hencheck, J. D. Hinnefeld, G. F. Peaslee, A. L. Fritsch, C. Hall, U. Khadka, Patrick J. Mears, P. O'Rourke, D. Padilla, J. Rieth, Tabatha Spencer and T. Williams, Phys. Rev. C **75**, 031302(R) (2007).

[23] N. Keeley, J. M. Cook, K. W. Kemper, B. T. Roeder and W. D. Weintraub, Phys. Rev. C **68**, 054601 (2003).

[24] R. S. Machintosh and N. Keeley, Phys. Rev. C **70**, 024604 (2004).

[25] N. Keeley and R. S. Machintosh, Phys. Rev. C **71**, 057601 (2004).

[26] T. Matsumoto, T. Egami, K. Ogata, Y. Iseri, M. Kamimura and M. Yahiro, Phys. Rev. C **73**, 051602(R) (2006).

[27] L. F. Canto, P. R. S. Gomes, R. Donangelo and M. S. Hussein, Phys. Rep. **424**, 1 (2006).

[28] L. F. Canto, R. Donangelo and P. Lotti, Phys. Rev. C **52**, 2848(R) (1995).

[29] A. M. Sanchez-Benitez, D. Escrig, M. A. G. Alvarez, M. V. Andres, C. Angulo, M. J. G. Borge, J. Cabrera, S. Cherubini, P. Demaret, J. M. Espino, P. Figuera, M. Freer, J. E. Garcia-Ramos, J. Gomez-Camacho, M. Gulino, O. R. Kakuee, I. Martel, C. Metelko, A. M. Moro and F. Perez-Bernal, Nucl. Phys. A **803**, 30 (2008).

[30] E. A. Benjamim, A. Lepine-Szily, D. R. Mendes Junior, R. Lichtenthaler, V. Guimaraes, P. R. S. Gomes, L. C. Chamon, M. S. Hussein, A. M. Moro, A. Arazi, I. Padron, J. Alcantara Nunez, M. Assuncao, A. Barioni, O. Camargo Jr. , R. Z. Denke, P. N. de Faria and K. C. C. Pires, Phys. Lett. B **647**, 30 (2007).

[31] A. Di Pietro, P. Figuera, F. Amorini, C. Angulo, G. Cardella, S. Cherubini, T. Davinson, D. Leanza, J. Lu, H. Mahmud, M. Milin, A. Musumarra, A. Ninane, M. Papa, M. G. Pellegriti, R. Raabe, F. Rizzo, C. Ruiz, A. C. Shotter, N. Soic, S. Tudisco and L. Weissman, Phys. Rev. C **69**, 044613 (2004).

[32] A. Chatterjee, A. Navin, A. Shrivastava, S. Bhattacharyya, M. Rejmund, N. Keeley, V. Nanal, J. Nyberg, R. G. Pillay, K. Ramachandran, I. Stefan, D. Bazin, D. Beaumel, Y. Blumenfeld, G. de France, D. Gupta, M. Labiche, A. Lemasson, R. Lemmon, R. Raabe, J. A. Scarpaci, C. Simenel, and C. Timis, Phys. Rev. Lett. **101**, 032701 (2008).

[33] R. J. Smith, J. J. Kolata, K. Lamkin, A. Morsad, K. Ashktorab, F. D. Becchetti, J. A. Brown, J. W. Janecke, W. Z. Liu and D. A. Roberts, Phys. Rev. C **43**, 761 (1991).

[34] M. Milin, S. Cherubini, T. Davinson, A. Di Pietro, P. Figuera, . Miljani, A. Musumarra, A. Ninane, A. N. Ostrowski, M. G. Pellegriti, A. C. Shotter, N. Soi, C. Spitaleri and M. Zadro, Nucl. Phys. A **730**, 285 (2004).

[35] I. Boztosun, M. Karakoc and Y. Kucuk, Phys. Rev. C **77**, 064608 (2008).

[36] G. R. Satchler, *Direct Nuclear Reactions* (Oxford University Press, Oxford, 1983).

[37] Y. Kucuk and I. Boztosun, Nucl. Phys. A **764**, 160 (2006).

[38] D. M. Brink and N. Takigawa, Nucl. Phys. A **279**, 159 (1977).

[39] I. Boztosun, Phys. Rev. C**66**, 024610 (2002).

[40] I. J. Thompson, Computer Phys. Rep. **7**, 167 (1988).

	E	χ^2/N	σ_R	J_V	J_W		E	χ^2/N	σ_R	J_V	J_W
	MeV		mb	$MeVfm^3$	$MeVfm^3$		MeV		mb	$MeVfm^3$	$MeVfm^3$
^{12}C	8.79	4.76	1241.	256.24	90.91	^{27}Al	9.5	1.14	1237.	193.22	70.87
	9.18	2.52	1262.	256.79	90.14		11.0	1.61	1380.	194.71	68.42
	18.0	26.30	1453.	268.90	69.75		12.0	4.25	1453.	195.71	66.82
							13.4	2.29	1531.	197.12	64.58
^{64}Zn	10.0	0.40	537.5	155.73	62.35	^{65}Cu	22.6	36.27	2012.	163.95	46.53
^{58}Ni	9.0	1.63	383.1	158.63	64.73	^{197}Au	27.0	13.12	1925.	141.2	46.70
							40.0	0.51	2843.	148.88	35.94
^{208}Pb	14.0	0.75	3.935	132.69	57.39	^{209}Bi	14.7	19.87	9.190	133.25	67.10
	16.0	3.11	59.71	133.85	55.76		16.3	14.93	64.01	134.15	55.85
	18.0	3.23	302.3	135.02	54.12		17.8	11.40	235.7	135.05	54.60
	22.0	5.05	1118.	137.34	50.85		19.0	2.27	454.6	135.70	53.62
	27.0	5.70	1892.	140.71	46.82		22.5	2.25	1168.	137.78	50.74

TABLE I: The reaction cross section, volume integrals and χ^2/N values obtained by using the experimental error bars.

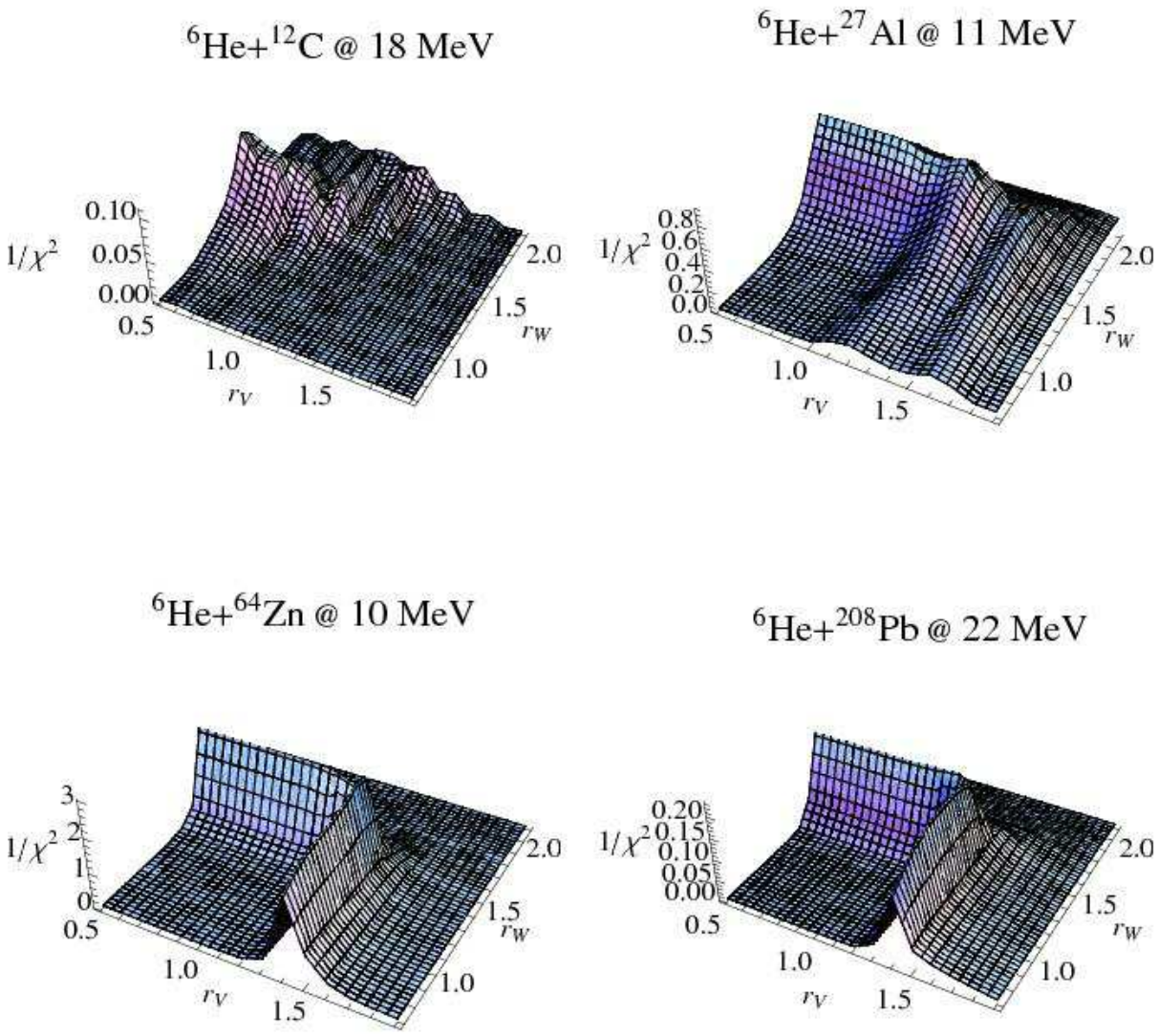


FIG. 1: (Color online) Three-dimensional plots of the optical model parameters r_V , r_W versus $1/\chi^2$, where χ^2 has the usual definition and measures the quality of the fit.

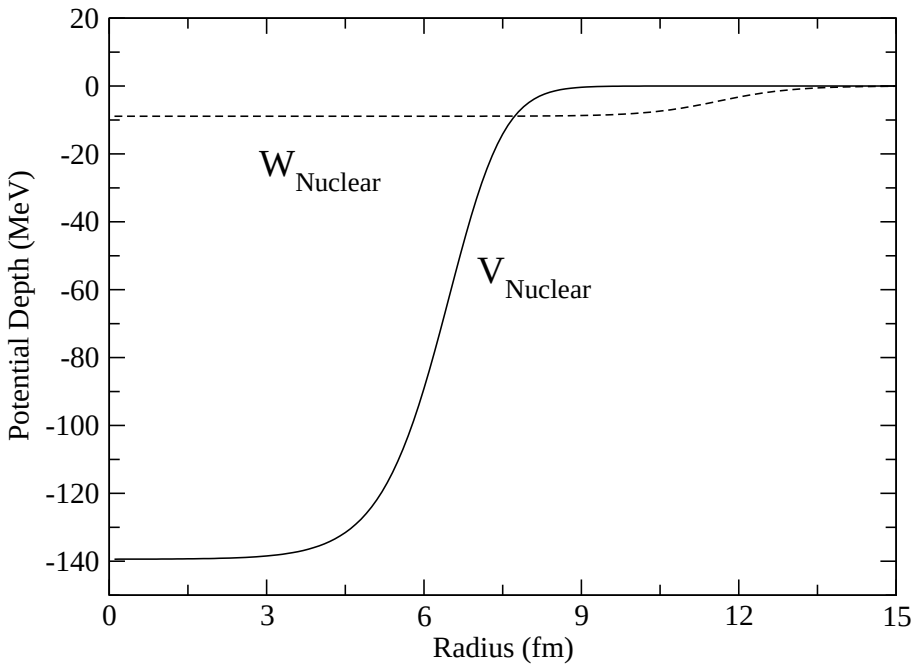


FIG. 2: The real (solid line) and imaginary parts (dashed line) of the nuclear potential at E_{Lab}=18 MeV for ^{6}He + ^{208}Pb.

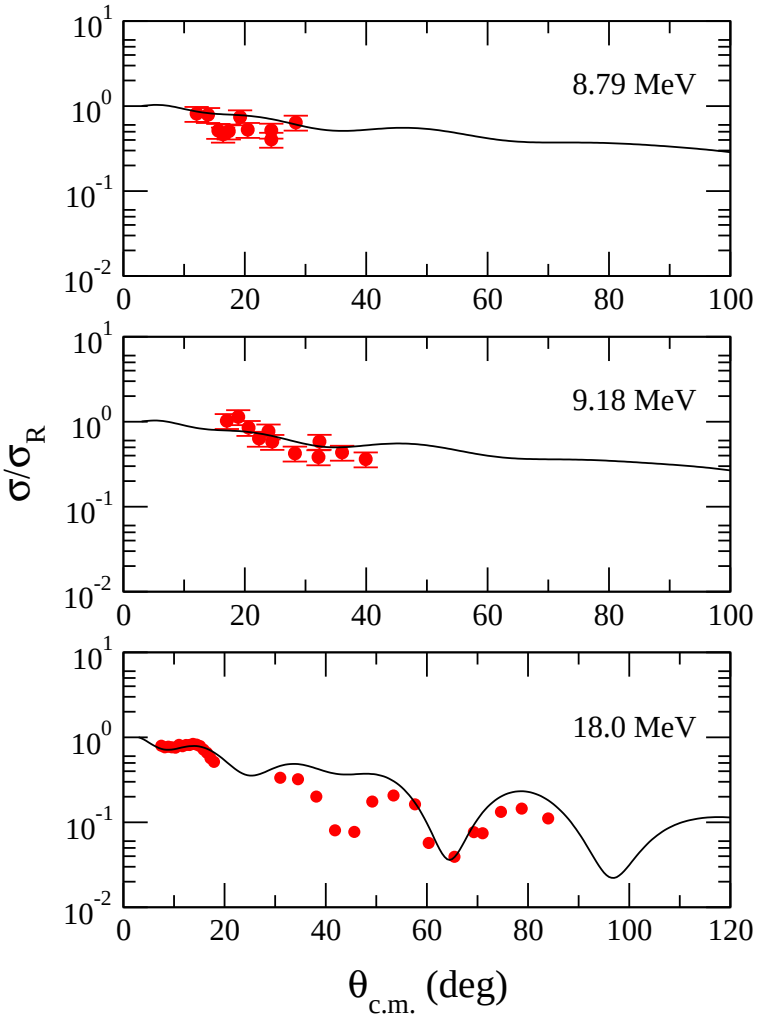


FIG. 3: (Color online) Elastic scattering angular distributions for ^{6}He + ^{12}C. The solid lines show OM calculation results while the circles show the experimental data. The experimental data have been taken from Ref. [33] and [34].

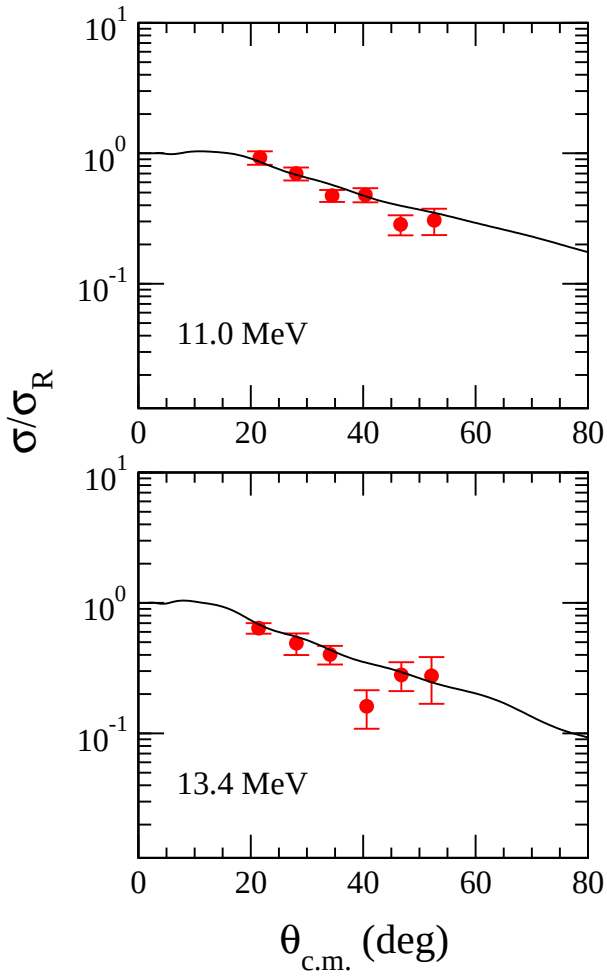


FIG. 4: (Color online) Elastic scattering angular distributions (ratio to Rutherford cross section) for ^{6}He + ^{27}Al. The solid lines show OM calculation results while the circles show the experimental data. The experimental data have been taken from Ref. [30].

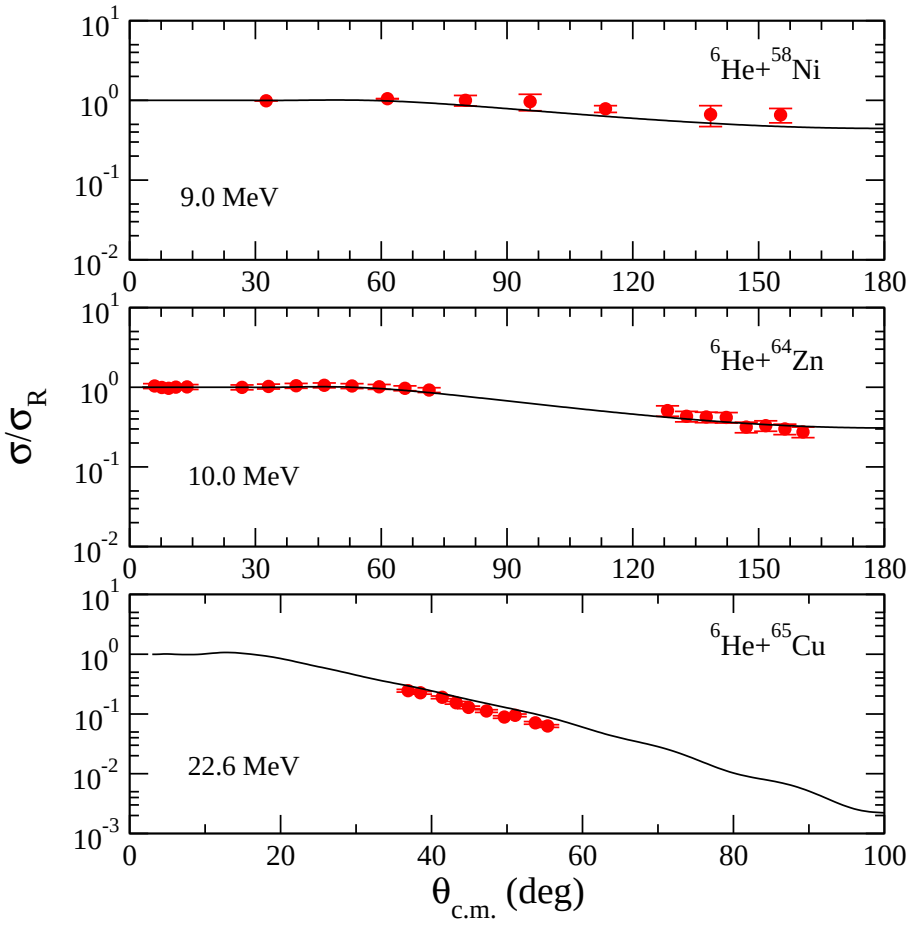


FIG. 5: (Color online) Elastic scattering angular distributions (ratio to Rutherford cross section) for ^{6}He + ^{58}Ni, ^{64}Zn, ^{65}Cu. The solid lines show OM calculation results while the circles show the experimental data. The experimental data have been taken from Ref. [17, 18, 31] and [32].

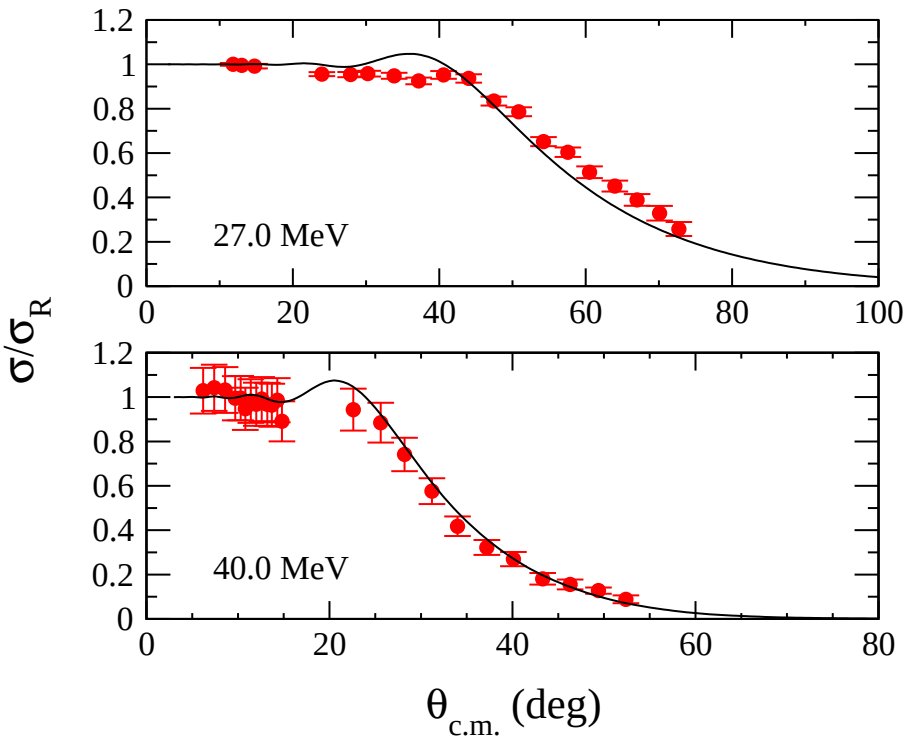


FIG. 6: (Color online) Elastic scattering angular distribution (ratio to Rutherford cross section) for ^{6}He + ^{197}Au. The solid lines show OM calculation results while the circles show the experimental data. The experimental data have been taken from Ref. [12] and [14].

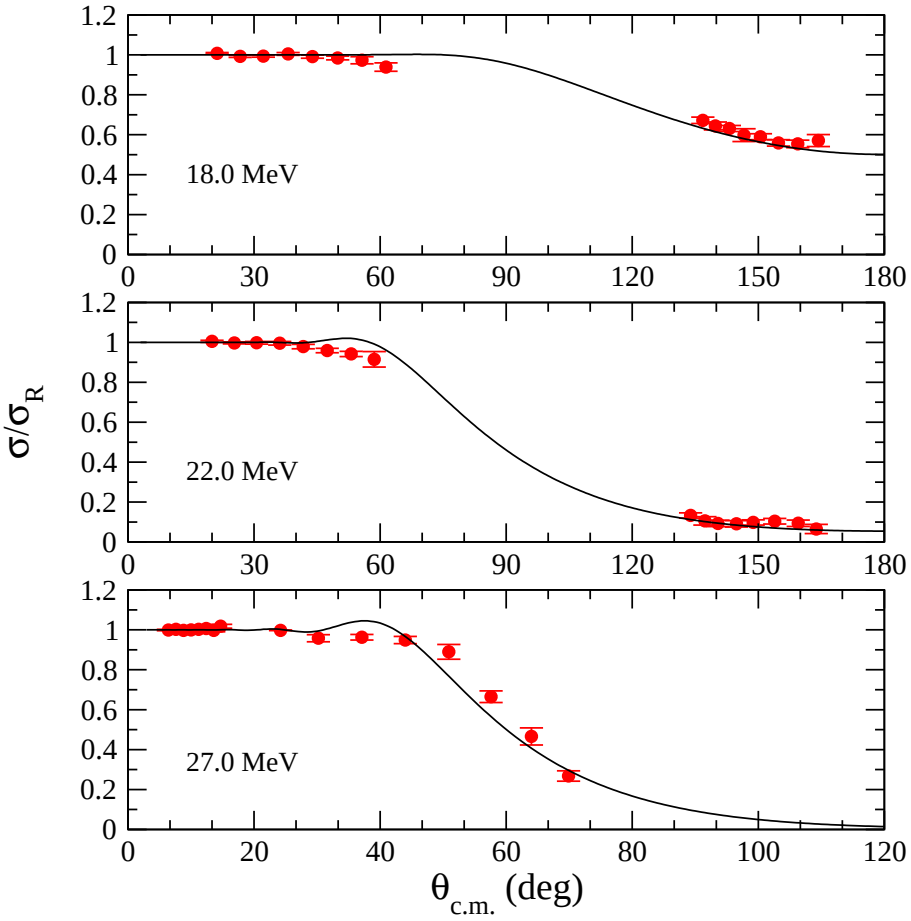


FIG. 7: (Color online) Elastic scattering angular distribution (ratio to Rutherford cross section) for ^{6}He + ^{208}Pb. The solid lines show OM calculation results while the circles show the experimental data. The experimental data have been taken from Ref. [8] and [13].

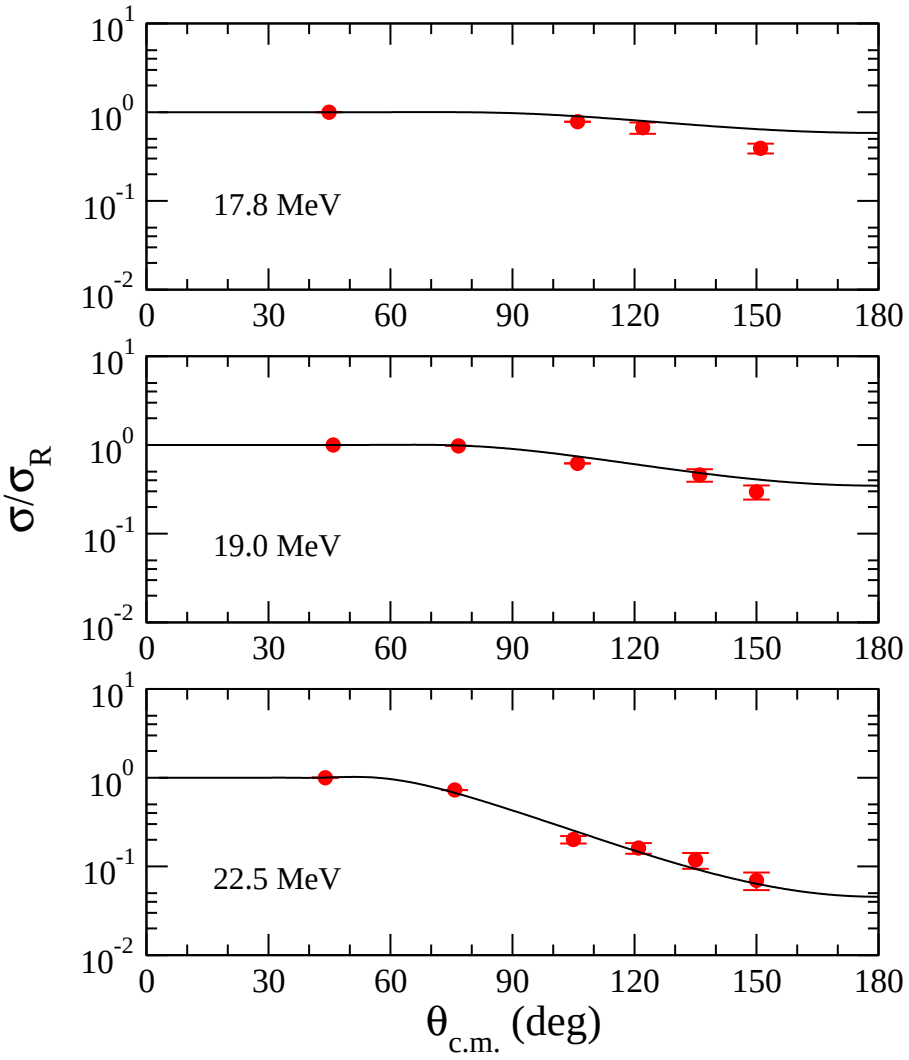


FIG. 8: (Color online) Elastic scattering angular distribution (ratio to Rutherford cross section) for ^{6}He + ^{209}Bi. The solid lines show OM calculation results while the circles show the experimental data. The experimental data have been taken from Ref. [9] and [10].

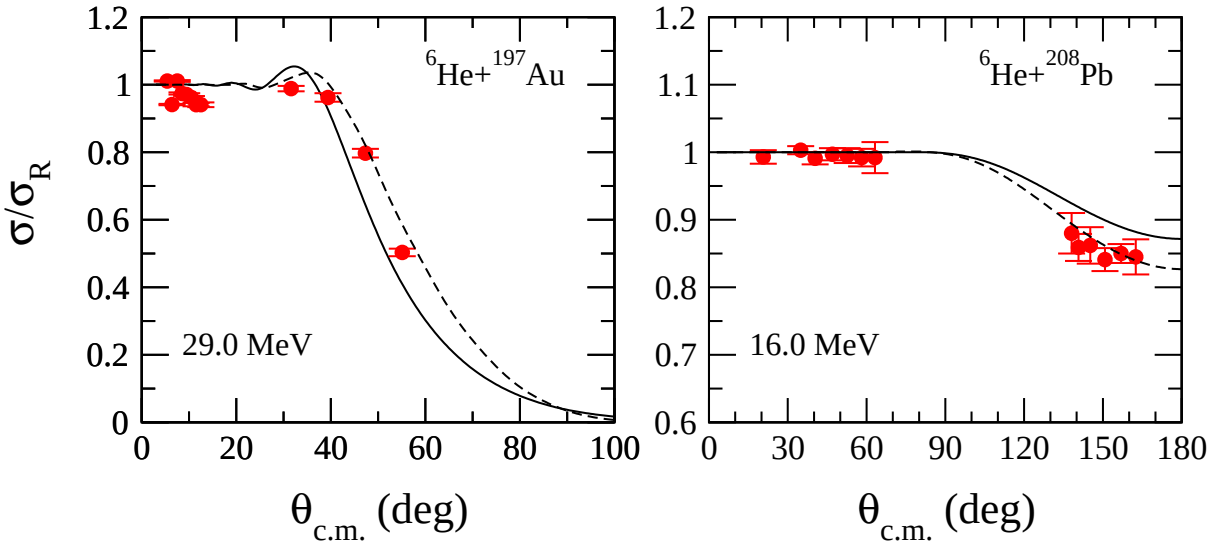


FIG. 9: (Color online) Elastic scattering angular distribution (ratio to Rutherford cross section) for ^{6}He + ^{197}Au and ^{6}He + ^{208}Pb. The solid lines show OM calculation results with the imaginary potential of Eq. 7 while the dashed lines show a decrease (left panel) and an increase (right panel) of 5 MeV from the value of Eq. 7.